

On the scaling properties of the total γ^*p cross section

M.N. Mondragon and J.G. Contreras

*Departamento de Física Aplicada, Centro de Investigación y Estudios Avanzados del I.P.N.,
97310, Mérida, Yucatán, México.*

Recibido el 31 de julio de 2006; aceptado el 4 de septiembre de 2006

We perform a detailed analysis on the scaling properties of the total γ^*p cross section, σ_{γ^*p} . We write the cross section as a product of two functions W and V representing, respectively, the dynamical degrees of freedom and the contribution from the valence partons. Analyzing data from HERA and fixed target experiments, we find that V is independent of Q^2 and concentrated at large x , while W carries all the information on the Q^2 evolution of γ^*p . We define the reduced cross section $\tilde{\sigma}_{\gamma^*p} \equiv W = \sigma_{\gamma^*p}/V$, and show that it is very close to a generalized homogeneous function. This property gives rise to geometric scaling for $\tilde{\sigma}_{\gamma^*p}$ and it also explains the known geometric scaling of σ_{γ^*p} at low x . As a consequence of our *Ansatz*, we also obtain a compact parameterization of σ_{γ^*p} describing all data above $Q^2 = 1 \text{ GeV}^2$.

Keywords: Deep Inelastic Scattering; Geometric Scaling

Hemos realizado un análisis detallado de las propiedades de escalamiento de la sección eficaz total σ_{γ^*p} . Escribimos esta sección eficaz como el producto de dos funciones, W y V , las cuales representan, respectivamente, los grados de libertad dinámicos y la contribución de los partones de valencia. Usando datos de HERA y de experimentos de blanco fijo, encontramos que V es independiente de Q^2 y se concentra a x grandes, mientras que W contiene toda la información de la evolución con Q^2 . Definimos la sección eficaz reducida $\tilde{\sigma}_{\gamma^*p} \equiv W = \sigma_{\gamma^*p}/V$, y demostramos que es muy similar a una función homogénea generalizada. Esta propiedad origina escalamiento geométrico para $\tilde{\sigma}_{\gamma^*p}$ y explica el escalamiento geométrico conocido de σ_{γ^*p} a x pequeña. Como consecuencia de nuestro *Ansatz*, obtenemos también una parametrización compacta de σ_{γ^*p} , la cual describe todos los datos arriba de $Q^2 = 1 \text{ GeV}^2$.

Descriptores: Dispersión inelástica profunda; Escalamiento geométrico

PACS: 13.60.Hb

1. Introduction

It has been found that, for small values of the Bjorken variable x , $x \leq 0.01$, the total γ^*p cross section, $\sigma_{\gamma^*p}(x, Q^2)$, extracted from lepton–hadron scattering experiments, presents the property of geometric scaling [1,2]. This property us permits to write the cross section as a function of only one variable, τ , called the scaling variable, which is the product of two functions, one depending only on Q^2 and the other only on x . It has been suggested that, for σ_{γ^*p} , τ is given by Q^2/Q_s^2 with $Q_s^2 = Q_s^2(x)$ known as the “saturation scale”. Geometric scaling has also been observed in eA reactions [3], including charm production [4] and nucleus–nucleus collisions [5].

The observation that σ_{γ^*p} grows quite rapidly at small x and that this behavior cannot continue indefinitely without violating the unitarity of the cross section led to the proposal of nonlinear QCD equations containing saturation [6–11]. One of the features of this type of equation is the introduction of a scale, Q_s^2 , to signal the onset of saturation effects. Much of the excitement and advance in the understanding of perturbative QCD at small x in recent years comes from the discovery that some saturation equations imply geometric scaling at the saturation scale [12–15].

Originally, from the point of view of these equations, geometric scaling was expected to be valid only at the saturation scale. However since its discovery in data from deep inelastic scattering, it has been suggested that geometric scaling was more general than saturation. It is observed within a kinematic range extending far above the saturation scale, up to

values of photon virtuality of $Q^2 = 450 \text{ GeV}^2$ ($x < 0.01$). This generality motivated theoretical work to find the region where geometric scaling is expected, either in exact or approximate form. Studies [16–18] based on the BFKL Equation [19] supplemented with specific boundary conditions have found that there is an extended region of phase space above Q_s^2 and below a Q_{max}^2 in which approximated geometric scaling is still valid. It has been estimated that for HERA energies, Q_{max}^2 is of the order of 100 GeV^2 if $Q_s^2 = 1 \text{ GeV}^2$, and around 400 GeV^2 if $Q_s^2 = 4 \text{ GeV}^2$.

Above this new scale one expects a complete breakdown of geometric scaling, so that $\sigma_{\gamma^*p}(x, Q^2)$ cannot be written as a product of two functions, one depending only on x and the other only on Q^2 . Furthermore, as the concept of geometric scaling has been linked to saturation, none of these investigations expect geometric scaling to be valid at medium to large x and Q^2 where the density of partons is very small.

Here, we study in detail the scaling properties of the total γ^*p cross section and find that geometric scaling is related to the fact that for small x , σ_{γ^*p} is very close to a homogeneous function, specifically a power law in both x and Q^2 . We show that it is possible to define a reduced cross section, hereafter called $\tilde{\sigma}_{\gamma^*p}$, which isolates this power law behavior not only for the small, but also for the large x region and thus shows geometric scaling in the complete kinematic plane.

This document is organized as follows. In the next section, we show that it is possible to isolate the power law behavior in x of σ_{γ^*p} for all values of Q^2 and define the reduced cross section $\tilde{\sigma}_{\gamma^*p}$. In Sec. 3. we study the behavior of $\tilde{\sigma}_{\gamma^*p}$ and show that it is very close to a generalized homoge-

neous function. In Sec. 4. we discuss the implications of our findings regarding saturation and geometric scaling. We also present a compact parameterization of σ_{γ^*p} which describes all data above $Q^2 = 1 \text{ GeV}^2$. Finally, in Sec. 5. we briefly summarize our findings and present our conclusions.

2. Analysis of the x and Q^2 dependence of σ_{γ^*p}

First, we turn to the behavior of σ_{γ^*p} for small x . It is known that the experimental data at small x can be described at each value of Q^2 by a power law in x [22]. From the point of view of theory, this behavior is expected, for Q^2 big enough to justify the use of pQCD, from both the DLLA approximation [23], if the starting Q^2 value for the QCD evolution is taken sufficiently small (see for example [24]), and from the BFKL [19] evolution.

In fact, this behavior is also seen in studies of geometric scaling above the saturation scale. For concreteness we use the saturation scale $Q_s^2(x) \sim x^{-\lambda_{\text{GBW}}}$, with $\lambda_{\text{GBW}} = 0.288$, as defined by K. Golec-Biernat and M. Wüsthoff [21]. Staśto *et al.* [1] found that, for $\tau = Q^2/Q_s^2(x) \gg 1$, $\sigma_{\gamma^*p}(\tau) \sim 1/\tau$, suggesting a power law behavior of σ_{γ^*p} as a function of x for constant values of Q^2 .

In summary, it is expected both from theory and phenomenology, and confirmed by experiment that, for small x , σ_{γ^*p} behaves like a power law for fixed values of Q^2 . Following these results, we propose to write the total γ^*p cross section at each Q^2 value as the product of two functions W and V :

$$\sigma_{\gamma^*p} = WV \quad (1)$$

where

$$W = Nx^{-\lambda}. \quad (2)$$

Note that in Equation (2), both the normalization N and the exponent λ may be different, for different values of Q^2 ; *i.e.*, $N = N(Q^2)$ and $\lambda = \lambda(Q^2)$.

As we are interested in isolating the scaling behavior of the cross section, we require V to be approximately constant for small x , so that it does not alter the physics embodied in W , and so that it describes the cross section for large x . It turns out that these requirements are very close to those expected from a valence distribution. Thus, for V , we tried a Gaussian functional form inspired by the model of Edin and Ingelman [25, 26].

In their model, the probe resolving the hadron has a much higher resolution than the size of the hadron, so that it sees free quarks and gluons in quantum fluctuations of the hadron. The momentum distributions of the partons are assumed to be Gaussian functions, to take into account the many small momentum transfers affecting the parton through the non-perturbative bound state interactions which cannot be calculated properly. Constraints are imposed to ensure kinematically allowed final states. Finally, they obtain a simple analytical expression in the approximation of small parton masses

and transverse momenta. Following their work, we propose

$$V = \exp\left(-\frac{(x-x_0)^2}{4\sigma^2}\right) \text{erf}\left(\frac{1-(x-x_0)}{2\sigma}\right), \quad (3)$$

where the Gaussian distribution represents the average of many random collisions that tie the valence parton to the hadronic bound state, and the error function takes care of enforcing the different kinematic constraints.

We proceed now to test the *Ansatz* embodied in Eqs. (1)-(3). We use data from fixed target [27] and HERA [28, 29] experiments. We chose Q^2 values such that there are measurements from both fixed target and HERA experiments, either at the same or at very similar Q^2 . The chosen values cover the range from 10 to 100 GeV^2 .

Normally, the Q^2 values from HERA and fixed target experiments are slightly different. We correct the fixed target data to the HERA values using the H1 PDF 2000 fit [28]. In most cases the correction factors are at the per mil level with a few cases at the one and two percent level. We then fit the data to the functional form of Eq. (1) for each Q^2 value. As an example, Fig. 1 shows data from HERA and fixed target experiments at $Q^2=12 \text{ GeV}^2$ and $Q^2=120 \text{ GeV}^2$ along with the result of the fit.

The data in Fig. 1 is very well described by Eq. (1). Furthermore, the same can be said at each value of Q^2 where there are measured points from both fixed target and HERA

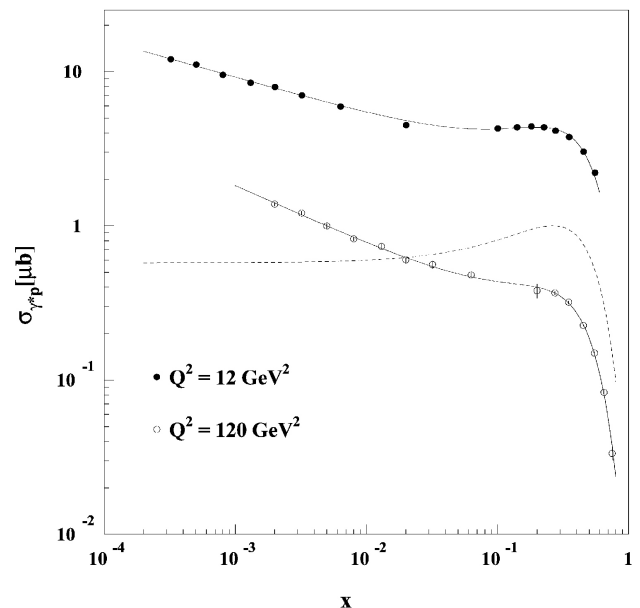


FIGURE 1. The total γ^*p cross section is shown as a function of x for $Q^2=12 \text{ GeV}^2$ and $Q^2=120 \text{ GeV}^2$. The points are experimental data from fixed target and HERA experiments and the solid line is a fit to the form of Eqs. (1)–(3). A power law is clearly seen for small values of x , while the structure at large x corresponds to a Gaussian-like distribution. The dashed line shows the contribution of the function $V(x)$ given in Eq. (3). Note that it is basically constant for small x and defines the shape of the curves for large x .

experiments. We find that all the x_0 extracted from the fit to Eq. (3) for the different Q^2 points available have numerical values consistent with each other within the errors. The same is true for the extracted values of the parameter σ . It follows then that V do not depend on Q^2 . We fit the different values of x_0 and σ each to a constant to obtain the $x_0 = 0.27$ and $\sigma^2 = 0.036$. We checked that using the extreme values of x_0 (0.26 and 0.28) and of σ^2 (0.032 and 0.04) does not change the results of the analysis. The function V with these mean values of the parameters x_0 and σ is also shown in Fig. 1. Note that V is basically constant for $x \lesssim 0.01$ and only contributes to the shape of the cross section above this value.

The fact that V can be taken independently of Q^2 implies that the QCD evolution in Q^2 of the cross section is solely contained in W . Thus, we define, in the complete kinematic plane, the reduced cross section $\tilde{\sigma}_{\gamma^*p}$ as

$$\tilde{\sigma}_{\gamma^*p} \equiv W(x, Q^2) = \sigma_{\gamma^*p}/V(x). \quad (4)$$

3. Analysis of the behavior of $\tilde{\sigma}_{\gamma^*p}$

We turn now to the study of the reduced cross section defined in Eqs. (2) and (4). Specifically, we study the dependence on Q^2 of both N and λ . We use all HERA data [28, 29] to fit $\tilde{\sigma}_{\gamma^*p}$ for fixed values of Q^2 . We do not use fixed target

data at this stage of the analysis, because those data points are concentrated at large x and thus, they do not have a lever arm long enough to determine accurately the power law parameters. Their influence has already been taken into account through $V(x)$.

We use 40 different experimental values Q^2 , ranging from 0.15 to 8000 GeV^2 , with enough data points in x to perform the fit. The average number of points for each fit was 8, ranging from 5 to 12. At each value of Q^2 , Eq. (2) provides an excellent description of data. The results for N and λ for each individual fit are quite precise and provide a clear picture of their dependence on Q^2 as shown in Fig. 2. Note that for the small x region this behavior has been predicted in Ref. 30 and, also for the small x region, has already been observed [22].

We observe a dramatic change in the behavior of both functions, $N(Q^2)$ and $\lambda(Q^2)$, when the virtuality of the photon approaches from above the region below 1 GeV^2 . Here λ is, as expected, very similar to that found with the Donnachie–Landshoff parameterization [31], while the normalization appears to saturate. Furthermore, the values of N and λ for the Q^2 data below 1 GeV^2 are almost constant in comparison to the steep dependence of these functions above 1 GeV^2 .

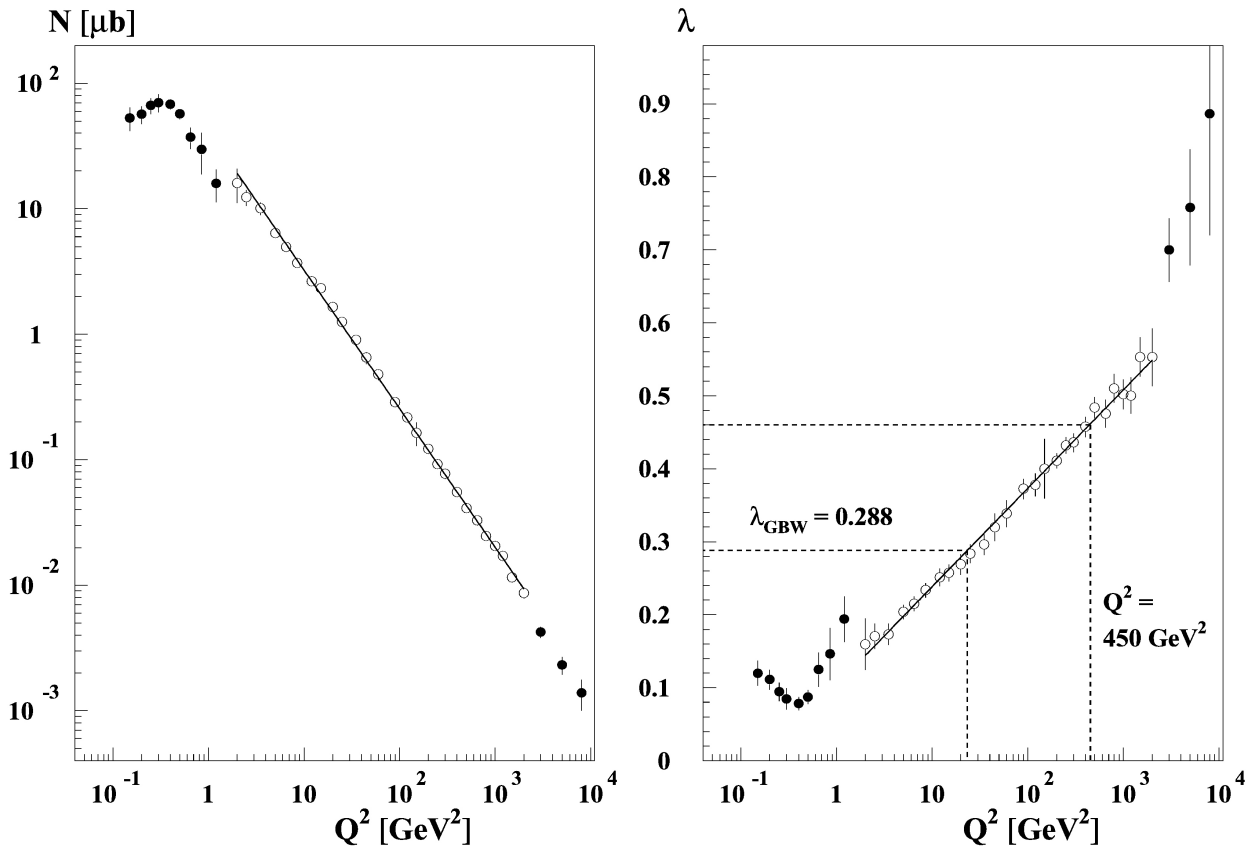


FIGURE 2. The dependence of Q^2 on the normalization N and the exponent λ of $\tilde{\sigma}_{\gamma^*p} = Nx^{-\lambda}$, extracted from fits of HERA data to the reduced cross section $\tilde{\sigma}_{\gamma^*p}$ at fixed values of Q^2 . The solid lines are fits to Eqs. (5) and (6) in the intermediate Q^2 range given by the empty bullets in the figure. The horizontal dash lines show the value of λ obtained by Golec-Biernat and Wuesthoff [21] as well as the highest Q^2 value of their analysis.

Above $Q^2 \approx 1 \text{ GeV}^2$, $\lambda(Q^2)$ can be described with the following functional form:

$$\lambda(Q^2) = \alpha \log_{10}(Q^2/\Lambda^2), \quad (5)$$

while $N(Q^2)$ behaves as the power law

$$N(Q^2) = \beta \left(\frac{Q^2}{Q_0^2} \right)^{-(1+\epsilon)}, \quad (6)$$

where Q_0^2 has been taken as 1 GeV^2 .

A fit in the intermediate Q^2 region to the data plotted in Fig. 2 yields $\beta = 41.0 \pm 1.5 \mu\text{b}$, $\epsilon = 0.103 \pm 0.007$, $\alpha = 0.135 \pm 0.003$ and $\Lambda^2 = 0.17 \pm 0.03 \text{ GeV}^2$. The quality of the fits is $\chi^2/dof = 0.66$ and $\chi^2/dof = 0.32$ for $N(Q^2)$ and $\lambda(Q^2)$ respectively. Note that the points at the largest Q^2 were not taken into account, because they have large fluctuations due to the limited statistics of data.

In summary, for Q^2 values below 1 GeV^2 the Q^2 dependence on W is very weak and the function depends mainly on one variable: x . Above 1 GeV^2 W , is very well described by the following functional form:

$$W(x, Q^2) = \beta \left(\frac{Q^2}{Q_0^2} \right)^{-(1+\epsilon)} x^{-\alpha \log_{10}(Q^2/\Lambda^2)}. \quad (7)$$

4. Discussion

Scaling. The dependence of Q^2 on λ is only logarithmic. Consider first the case where the exponent of x is a constant, $\lambda = \lambda_0$. Naming W_0 the function W with λ_0 , Eq. (7) would be of the form

$$W_0(x, Q^2) = k(Q^2)^{-(1+\epsilon)} x^{-\lambda_0}, \quad (8)$$

where k is just the normalization.

In this case W_0 is a generalized homogeneous function, which, as can easily be demonstrated, implies that for all t real and greater than zero, the following equation is valid:

$$W_0(t^{-1/\lambda_0} x, t^{1/(1+\epsilon)} Q^2) = W_0(x, Q^2). \quad (9)$$

In particular, it is also valid for $t = x^{\lambda_0}$:

$$W_0|_{t=x^{\lambda_0}}(1, x^{\lambda_0/(1+\epsilon)} Q^2) \equiv W_0(\tau_0) = W_0(x, Q^2); \quad (10)$$

i.e., W_0 exhibits *exact* geometric scaling behavior with the scaling variable given by $\tau_0 = x^{\lambda_0/(1+\epsilon)}(Q/Q_0)^2$.

Now, we turn to the real case where λ depends on Q^2 . Here we find that

$$W(x, Q^2) = W_0(x, Q^2) x^\delta, \quad (11)$$

where

$$\delta(Q^2) \equiv \lambda_0 - \alpha \log_{10}(Q^2/\Lambda^2). \quad (12)$$

Note that $W(x, Q^2)$ can be written as the product of a generalized homogeneous function, for which geometric scaling is exactly valid, and the factor x^δ . This last factor embodies the violations to geometric scaling. It turns out that due to the limited phase space where data are currently available, the factor x^δ for a fixed x does not change much and thus the reduced cross section $W(x, Q^2)$ is suppressed by a numerically similar factor for all values of Q^2 at a given x . Furthermore, the factor x^δ varies smoothly as a function of τ so that the geometric scaling behavior is kept, albeit in an approximate fashion, for all values of x and Q^2 as shown in the left panel of Fig. 3.

This reasoning is also valid for the kinematic region studied by Stařto et al., because, given that the function $V(x)$ is basically a constant for $x \lesssim 0.01$, the total cross section σ_{γ^*p} is proportional to $W(x, Q^2)$. Thus, for the low x region, σ_{γ^*p} can also be written as a product of a generalized homogeneous function and the x^δ factor as in Eq. (11).

The left panel of Fig. 3 shows the measured reduced cross section scaled by the factor $x^{-\delta}$ as a function of τ_0 to demonstrate that, when the violation of geometric scaling is taken into account, the data show a power law behavior over the entire available kinematic plane.

It is quite interesting to compare Fig. 3 with Fig. 4. The latter figure contains all data points above $Q^2 = 1 \text{ GeV}^2$ before the data collapse produced by the transformation to the scaling variable τ . The comparison of both figures shows that the collapse of all data in a single line is not a trivial fact.

Power laws, scaling and critical phenomena. It must be emphasized that the origin of scaling within this approach is the fact that W is very close to a generalized homogeneous function. This fact is valid even for very large values of x , where one would not necessarily expect saturation effects to be present. But it does not exclude the possibility that the mechanism which gives rise to the power law behavior of W is also linked to saturation.

In this context, it is interesting to note that scaling and its relation to power laws has been widely discussed in relation to critical phenomena. In particular it has been found that under some conditions the presence of a renormalization group equation helps to explain the appearance of power laws, and of its associated scaling, and permits us also to explain and numerically estimate the appearance of scaling violations (see for example [32, 33] and references therein).

It is interesting to note that the power law behavior of the total γ^*p cross section is generated by the branching process embodied in QCD evolution equations which are in fact a type of renormalization group equations. Also the case of saturation has been cast, within the Color Glass Condensate approach [9], in the form of renormalization group equations. It is clear then, that the goal of finding a deeper understanding of the relation between renormalization group equations and the emergence of power laws in pQCD deserves further study.

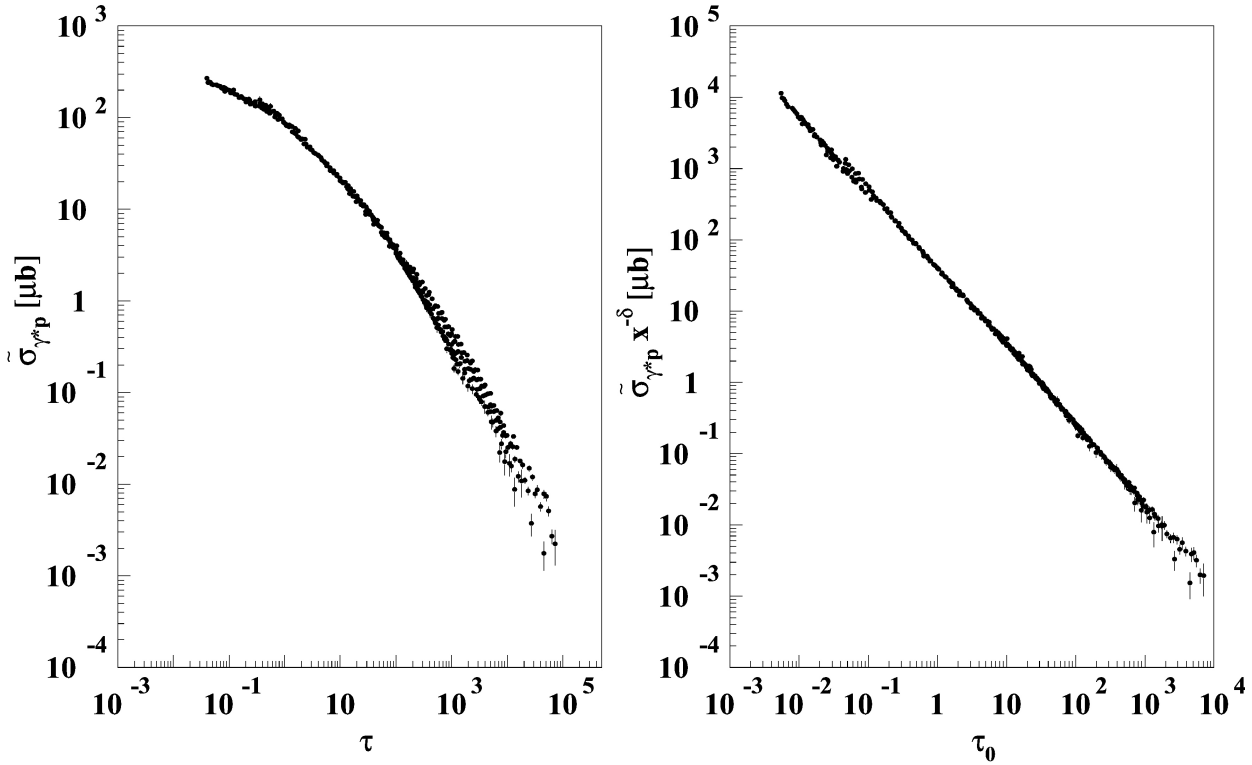


FIGURE 3. The left panel shows the reduced γ^*p cross section, $\tilde{\sigma}_{\gamma^*p}$, as a function of the scaling variable $\tau = Q^2/Q_s^2$ [21] for all data in Refs. 27 to 29. The geometric scaling behavior is clearly seen for all values of τ . The right panel shows the data corresponding to the reduced cross section, scaled by the factor x^δ responsible for the violations of scaling according to the model of Eqs. (11) and (12) with $\lambda_0 = \lambda_{GBW}$. One observes a power law behavior over many orders of magnitude covering all the available phase space.

A parameterization of σ_{γ^*p} above $Q^2 = 1 \text{ GeV}^2$. Note that as a consequence of the description of σ_{γ^*p} given by Eq. (1) we also have a simple six parameter description of the total γ^*p cross section for *all* Q^2 values above 1 GeV^2 :

$$\sigma_{\gamma^*p}(x, Q^2) = \beta \left(\frac{Q^2}{Q_0^2}\right)^{-(1+\epsilon)} x^{-\alpha \log_{10}(Q^2/\Lambda^2)} \times \exp\left(-\frac{(x-x_0)^2}{4\sigma^2}\right) \text{erf}\left(\frac{1-(x-x_0)}{2\sigma}\right). \quad (13)$$

Equation (13) is compared to data in Fig. 4 using the parameters obtained from the fit to Fig. 3. For these parameters the χ^2/dof obtained for $Q^2 > 1 \text{ GeV}^2$ is $\chi^2/dof = 0.77$.

5. Summary and conclusions

We have shown that, for any Q^2 , σ_{γ^*p} can be factorized as a product of a power law function, $W(x, Q^2)$, which dominates at small x and a Gaussian-like distribution, $V(x)$, which is important at large x . We have found that W carries all the information on Q^2 evolution, whereas V depends only on x . The dynamical power law behavior is isolated by defining a reduced cross section $\tilde{\sigma}_{\gamma^*p} = \sigma_{\gamma^*p}/V = W$.

In turn, we have shown that W factorizes as the product of a generalized homogeneous function, $W_0(x, Q^2)$, with the property of exact geometric scaling, and a factor $x^{\delta(Q^2)}$, responsible for the violations to geometric scaling. This property, along with the limited phase space available in data, is

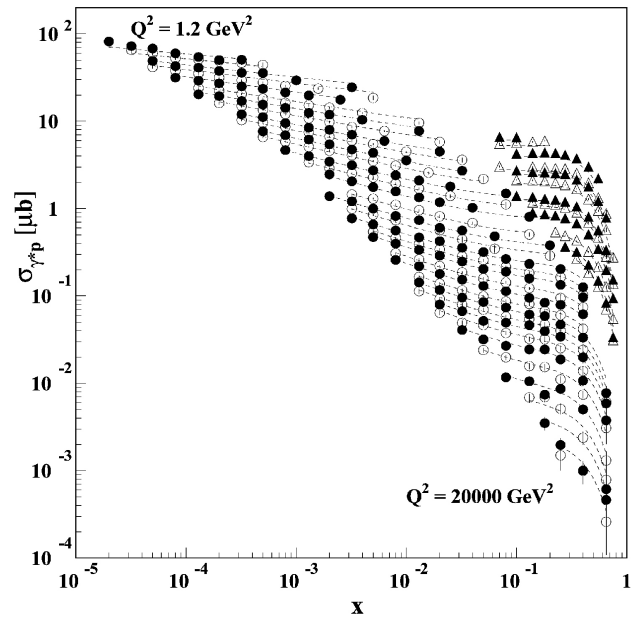


FIGURE 4. The total γ^*p cross section, σ_{γ^*p} , is shown as a function of x for different fixed values of Q^2 going from $Q^2=1.2 \text{ GeV}^2$ to $Q^2=20000 \text{ GeV}^2$. The bullets are the experimental data points from HERA, while the triangles are from fixed target experiments. The alternation of full and empty symbols is just to get a clear display of data. The lines are the result of Eq. (13).

found to be responsible for the geometric scaling behavior of $\tilde{\sigma}_{\gamma^*p}$ as well as of σ_{γ^*p} , because $\sigma_{\gamma^*p} \sim \tilde{\sigma}_{\gamma^*p}$ in the small x region.

These results show that the emergence of geometric scaling is not necessary related to the low x region, nor to saturation and open up interesting possibilities for further studies of the relation between evolution equations and the appearance of scaling behavior in QCD.

Finally, as a consequence of our studies we obtained a six parameter description of all σ_{γ^*P} data above $Q^2 \approx 1 \text{ GeV}^2$, where each parameter has a natural physical interpretation.

Acknowledgments

This work has been partially supported by the Conacyt grant 40073-F.

-
1. A.M. Staśto, K. Golec-Biernat, and J. Kwieciński, *Phys. Rev. Lett.* **86** (2001) 596.
 2. Schildknecht, B. Surrow, and M. Tentyukov, *Phys. Lett. B* **499** (2001) 116.
 3. A. Freund, K. Rummukainen, H. Weigert, and A. Schäfer, *Phys. Rev. Lett.* **90** (2003) 222002.
 4. V. P. Goncalves and M.V.T. Machado, *Phys. Rev. Lett.* **91** (2003) 202002.
 5. N. Armesto, C.A. Salgado, and U.A. Wiedemann, *Phys. Rev. Lett.* **94** (2005) 022002.
 6. L.V. Gribov, E.M. Levin, and M.G. Ryskin, *Phys. Rep.* **100** (1983) 1.
 7. E.M. Levin and M.G. Ryskin, *Phys. Rep.* **189** (1990) 267.
 8. A.H. Mueller and J. Qiu, *Nucl. Phys. B* **268** (1986) 427; J. P. Blaizot and A. H. Mueller, *Nucl. Phys. B* **289** (1987) 847.
 9. L. McLerran and R. Venugopalan, *Phys. Rev. D* **49** (1994) 2233; **49** (1994) 3352; **50** (1994) 2225.
 10. I. Balitsky, *Nucl. Phys. B* **463** (1996) 99.
 11. Yu. V. Kovchegov, *Phys. Rev. D* **60** (1999) 034008.
 12. J. Bartels and E. Levin, *Nucl. Phys. B* **387** (1992) 617.
 13. E. Levin and K. Tuchin, *Nucl. Phys. B* **573** (2000) 833; *Nucl. Phys. A* **691** (2001) 779; **693** (2001) 787.
 14. E. Iancu and L. McLerran, *Phys. Lett. B* **510** (2001) 145.
 15. S. Munier and R. Peschanski, *Phys. Rev. Lett.* **91** (2003) 232001.
 16. J. Kwieciński and A.M. Staśto, *Phys. Rev. D* **66** (2002) 014013;
 17. E. Iancu, K. Itakura, and L. McLerran, *Nucl. Phys. A* **708** (2002) 327.
 18. A.H. Mueller and D.N. Triantafyllopoulos, *Nucl. Phys. B* **640** (2002) 331; D.N. Triantafyllopoulos, *Nucl. Phys. B* **648** (2003) 293.
 19. E.A. Kuraev, L.N. Lipatov and V.S. Fadin, *Sov. Phys. JETP* **45**, 199 (1977); Ya.Ya. Balitsky and L.N. Lipatov, *Sov. J. Nucl. Phys.* **28**, 22 (1978).
 20. A.H. Mueller and A.I. Shoshi, *Nucl. Phys. B* **692** (2004) 175; E. Iancu, A.H. Mueller, and S. Munier, *Phys. Lett. B* **606** (2005) 342.
 21. K. Golec-Biernat and M. Wüsthoff, *Phys. Rev. D* **59** (1999) 014017; **60** (1999) 114023.
 22. H1 Collab. *et al.*, *Phys. Lett. B* **520** (2001) 183.
 23. A. de Rújula *et al.*, *Phys. Rev. D* **10** (1974) 1649.
 24. J. Kwieciński, *J. Phys. G.* **22** (1996) 685.
 25. A. Edin and G. Ingelman, *Phys. Lett. B* **432** (1998) 402.
 26. A. Edin and G. Ingelman, *Nucl. Phys. Proc. Suppl. B* **79** (1999) 189.
 27. BCDMS Collaboration, A.C. Benvenuti *et al.*, *Phys. Lett. B* **223** (1989) 485.
 28. H1 Collab., C. Adloff *et al.*, *Eur. Phys. J. C* **19** (2001) 269; **21** (2001) 33; **30** (2003) 1.
 29. ZEUS Collab, J. Breitweg *et al.*, *Phys. Lett. B* **487** (2000) 53.
 30. H. Navelet, R. Peschanski, and S. Wallon, *Mod. Phys. Lett. A* **9** (1994) 3393.
 31. A. Donnachie and P.V. Landshoff, *Phys. Lett. B* **296** (1992) 227.
 32. M. E. Fischer, *Rev. Mod. Phys.* **70** (1998) 653.
 33. K. G. Wilson, *Rev. Mod. Phys.* **55** (1983) 583.